# One-Step Coating of Full-Coverage CsPbBr Thin Films via Mist Deposition for All-Inorganic Perovskite Solar Cells

AUTHOR(S):

Haruta, Yuki; Ikenoue, Takumi; Miyake, Masao; Hirato, Tetsuji

CITATION:

Haruta, Yuki ...[et al]. One-Step Coating of Full-Coverage CsPbBr Thin Films via Mist Deposition for All-Inorganic Perovskite Solar Cells. ACS Applied Energy Materials 2020, 2020(3): 11523-11528

ISSUE DATE:

2020-12-28

URL:

http://hdl.handle.net/2433/263141

# One-Step Coating of Full-Coverage $CsPbBr_3$ Thin Films via Mist Deposition for All-Inorganic Perovskite Solar Cells

*Yuki Haruta, Takumi Ikenoue*, Masao Miyake, and Tetsuji Hirato*

Graduate School of Energy Science, Kyoto University, Kyoto 606-8501, Japan

*E-mail: ikenoue.takumi.4m@kyoto-u.ac.jp

## Abstract

In this work, one-step coating of $CsPbBr_3$ thin films using the mist deposition method is demonstrated. The $CsPbBr_3$ layer is composed of large grains with an average size of approximately 1.4 μm, and it fully covers the substrate surface, unlike the layers prepared by conventional one-step spin-coating methods, so that efficient carrier transport is realized. Carbon-based $CsPbBr_3$ perovskite solar cells (PSCs) fabricated using the mist deposition method exhibit a stabilized power conversion efficiency of 7.7%, which is a record value for carbon-based $CsPbBr_3$ PSCs prepared via a one-step solution process.

## Keywords

All-inorganic perovskite, Mist deposition, One-step solution process, Perovskite, Photovoltaics

## TOC GRAPHICS

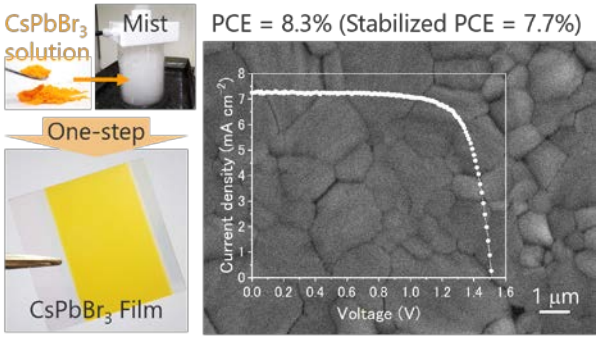

Organic–inorganic metal halide perovskites have attracted much attention as promising photoconductive layers for next-generation solar cells owing to their high absorption coefficients, high carrier mobilities, long carrier lifetimes, and easily tunable bandgaps.[1–4] However, the thermal and moisture instability of organic cations has impeded their further application.[5] Substituting the organic cations with $Cs^+$ is one of the most effective solutions to this stability problem. Among Cs-based perovskites, $CsPbBr_3$ has demonstrated a remarkably high stability against moisture and heat.[6,7] In addition, replacing the metallic electrode with a carbon electrode is also an effective way to improve the stability. Carbon-based perovskite solar cells (PSCs), which eliminate the need for precious metal electrodes and hole transport layers, have demonstrated improved stability and reduced fabrication cost.[8–10] Following this trend, new type PSCs incorporating extremely durable carbon electrodes and $CsPbBr_3$ were proposed and demonstrated great stability.[11] Owing to its reduced fabrication cost and high stability, this state-of-the-art PSC is one of the most practical PSCs.

Since the first carbon-based $CsPbBr_3$ PSCs were reported in 2016,[11] their power conversion efficiencies (PCEs) have improved from 6.7% to more than 10% through various efforts such as interface engineering[12–17] and compositional engineering.[18–20] Despite these attempts at improving the PCE, there has been insufficient progress in developing solution processes for their industrialization. Although $CsPbBr_3$ thin films have been prepared by two-step spin-coating methods involving $PbBr_2$ preparation and its subsequent conversion to $CsPbBr_3$ with a CsBr solution, these methods require precise compositional control to suppress the formation of impurity phases such as $Cs_4PbBr_6$ and $CsPb_2Br_5$ during the second step.[12] In contrast, simple one-step methods that can directly form $CsPbBr_3$ from the precursor solution is preferable for industrialization. In the one-step method, however, the $CsPbBr_3$ films often suffer from poor

coverage because the density of the heterogeneous nuclei tends to be low owing to the poor solubility of CsBr in typical organic solvents, such as dimethyl sulfoxide (DMSO).[21–24]

To increase the density of heterogeneous nuclei, Y. Ren *et al.* proposed a fast nucleation-deposition method by introducing polyethylene glycol (PEG) in a one-step solution.[23] They revealed that the PEG increases the cluster number of CsBr-$PbBr_2$-DMSO-PEG colloids in the solution. These colloids serve as a nucleation site and induce fast nucleation-deposition. Consequently, the surface coverage of the $CsPbBr_3$ film was drastically improved. The obtained $CsPbBr_3$-based PSCs achieved a stabilized PCE of 7.2%, which is the highest efficiency recorded in the one-step method.[23] However, the PCE is still lower than those in the case of the two-step methods. We cannot dismiss the possibility that although the improved film coverage should improve the PCE, the residual additives within the $CsPbBr_3$ films limited the photovoltaic performance.

Herein, we propose mist deposition as a one-step method to realize fast nucleation-deposition without any additives for the preparation of full-coverage $CsPbBr_3$ thin films. Figure 1 shows a schematic illustration of the proposed concept. In this method, the precursor solution is atomized into numerous mist particles by a 2.4 MHz ultrasonic vibration. Generally, such high frequency generates small and uniform mist particles with a size of 3 μm (volume ~14 fL)[25] which is much smaller than that of droplets generated by air-brush (> size: 50 μm, volume: ~65 pL).[26] Therefore, as soon as the mist particles contact a preheated substrate, solvent evaporation and consequent fast nucleation-deposition should occur. Based on this hypothesis, at the initial stage of the deposition process, the numerous mist particles reaching the substrate one after another should repeat numerous fast nucleation-deposition, leading to a high density of heterogeneous nuclei. At the second stage, i.e. when the following mist particles adhere to the existing crystals, the re-

dissolution and crystal grain growth should occur as reported in a previous study.[27] It is expected that the film coverage would improve gradually and full-coverage $CsPbBr_3$ films are finally obtained after repeated crystal grain growth and additional nucleation. In addition to the potential for full-coverage film formation, the widely accepted scalability of mist deposition is also advantageous for industrialization.[28–30]

In this work, we show a proof-of-concept for full-coverage $CsPbBr_3$ thin films from a one-step solution without any additives using the mist deposition method. The $CsPbBr_3$ layer fully covers the substrate surface and is composed of large grains with an average size of approximately 1.4 μm, which allows efficient carrier transport to be realized. $CsPbBr_3$ PSCs with the configuration of indium tin oxide (ITO)/$TiO_2$/$CsPbBr_3$/carbon are fabricated to verify the quality of the $CsPbBr_3$ thin films. Thanks to the improved film coverage, a high open-circuit voltage ($V_{OC}$) of 1.51 V is achieved. The obtained stabilized PCE of 7.7% is a record value for carbon-based $CsPbBr_3$ PSCs fabricated via a one-step solution process.

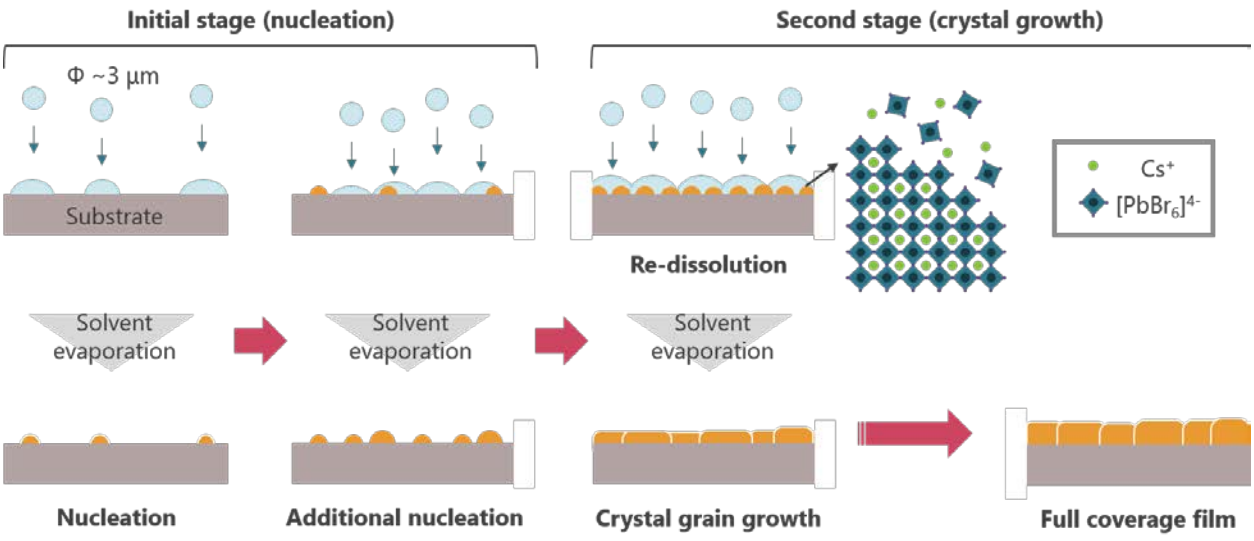


**Figure 1.** Schematic illustration of full coverage $CsPbBr_3$ film preparation by using mist deposition.

$CsPbBr_3$ films were first prepared on glass substrates by the mist deposition method (see the Supporting Information for experimental details). The precursor solution was prepared by dissolving $CsPbBr_3$ powder in a mixture of DMSO and *N*,*N*-dimethylformamide (DMF) (1:4, *v*/*v*). DMF was added to decrease the solvent viscosity and thus facilitate mist generation (Figure S1). The $CsPbBr_3$ concentration was determined to be 0.06 M considering that the maximum solubility of $CsPbBr_3$ in the DMSO–DMF mixed solvent was approximately 0.1 M (Figure S2). As shown in Figure 2a, a uniform $CsPbBr_3$ film was obtained on the glass substrate. The top-view scanning electron microscopy (SEM) image reveals that the $CsPbBr_3$ film fully covered the substrate surface without any voids (Figure 2b), unlike films prepared by the conventional one-step spin-coating method.[23] To investigate the optical properties and crystallinity, the absorbance spectrum and the X-ray diffraction (XRD) pattern were measured. Figure 2c shows the absorbance spectrum and the corresponding Tauc plot of the $CsPbBr_3$ film, which confirmed that the absorption edge and optical bandgap ($E_g$) were 527 nm and 2.35 eV, respectively, and were in agreement with previously reported values for $CsPbBr_3$.[11] As shown in Figure 2d, the XRD pattern was well matched to that of the orthorhombic $CsPbBr_3$ phase[31] with the preferred orientation along the (101) plane, which is consistent with our previous report.[32] Additionally, no changes were observed in the XRD pattern after storage for over 1 month under atmospheric conditions (0–25 °C, average RH 60%). The fact that peaks derived from an impurity phase, such as $Cs_4PbBr_6$ or $CsPb_2Br_5$, were not detected, shows that a high-purity $CsPbBr_3$ film was produced by the mist deposition method. In terms of chemical equilibrium theory, the Cs-rich impurity phase tends to precipitate from the solution in which Cs and Pb are dissolved in equal molar ratios[24]. However, in the case of the mist deposition method, $CsPbBr_3$, which has the same composition ratio as that of the solution, tends to precipitate because the solute is precipitated by fast evaporation of mist particles. These results

demonstrated that full-coverage $CsPbBr_3$ thin films can be obtained from a one-step solution without any additives by using the mist deposition method. Generally, voids in the photoconductive layer cause voltage loss owing to the formation of short-circuit.[33] Therefore, it is expected that the void-free $CsPbBr_3$ film could realize a high $V_{OC}$.

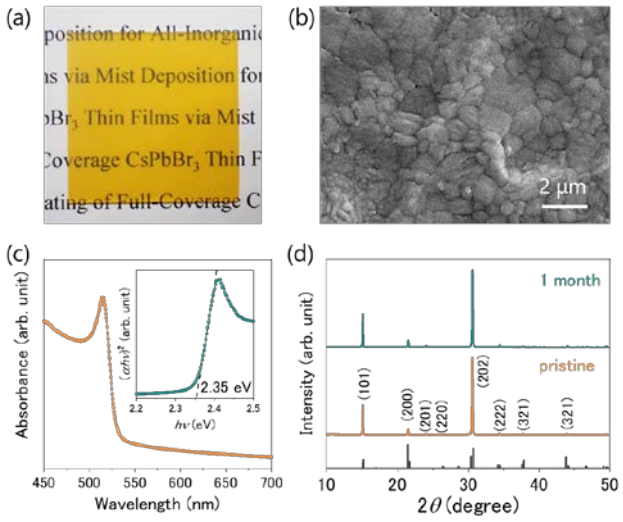


**Figure 2.** (a) Photograph (25 × 25 $mm^2$), (b) top-view SEM image, (c) absorbance spectrum (inset: Tauc plot) and (d) XRD patterns of the pristine $CsPbBr_3$ film and aged $CsPbBr_3$ film.

To evaluate the photovoltaic performances of the $CsPbBr_3$ thin films, $CsPbBr_3$ PSCs with the ITO/$TiO_2$/$CsPbBr_3$/carbon configuration were prepared. For photovoltaic application, not only the surface coverage ratio is important, but also the thickness of the photoconductive layer. Therefore, the thickness of the $CsPbBr_3$ film required to cover the substrate completely was investigated and the photovoltaic performances at various $CsPbBr_3$ thicknesses were evaluated. The $CsPbBr_3$ thickness was controlled by the stage speed ($v$) which is directly related to the amount of mist particles arriving at the substrate. Regardless of the stage speed, all detected XRD peaks were identified by $CsPbBr_3$ and the $TiO_2$/ITO substrate (Figure S3). Figure 3a and b show surface and cross-sectional SEM images of representative $CsPbBr_3$ PSCs, whereas Figure S4 and S5 show the

SEM images of the other PSCs. The film thickness and the grain size distribution (Figure S6) were measured from these SEM images. In the case of a too fast stage speed ($v$ = 0.12 mm $s^{-1}$ or above), the $CsPbBr_3$ layer only partially covered the substrate (Figure 3a), which was attributed to an insufficient amount of mist particles. By comparison, full-coverage was achieved at a moderate stage speed ($v$ = 0.04–0.08 mm $s^{-1}$) and the thickness was measured to be 340–920 nm (Figure 3b and S4). As shown in Figure 3c, the thickness and the mean grain size of the $CsPbBr_3$ layers increased in proportion to supply time, defined as the reciprocal of the stage speed. Additionally, the mean grain size was always more than twice the thickness. For the 580 nm thick $CsPbBr_3$ layer, the average grain size was 1.4 μm. Consequently, the $CsPbBr_3$ layer had a monolayer-vertical structure, which consisted of single grains arranged in a vertical direction, as shown in Figure 3b. This monolayer-vertical structure was also observed in the other full-coverage $CsPbBr_3$ layers (Figure S4). Figure 3d shows the photovoltaic performance, including the short-circuit current density ($J_{SC}$), $V_{OC}$, fill factor (FF), and PCE, of the $CsPbBr_3$ PSCs. It should be noted that full-coverage films were obtained when the thickness of the $CsPbBr_3$ layer was more than 340 nm (the area shown in yellow in Figure 3d). In the case of the poor coverage $CsPbBr_3$ layer, the average PCE was limited to 4.5%. By comparison, that of the full-coverage $CsPbBr_3$ layer drastically improved to 7.0–7.8%, which was attributed to especially the improved FF from 0.63 to 0.73–0.75 owing to the elimination of short-circuit. For the full-coverage layers, a high $V_{OC}$ of up to 1.51 V was obtained and the value is higher than those of the carbon-based PSCs in previous studies (Table S1). This fact suggests that the voltage loss was effectively eliminated by achieving full-coverage. Interestingly, the average PCEs at thicknesses of 580–920 nm distributed in a small range (7.6–7.8%). Considering that the increased photon absorption was negligible in this range (Figure S7), the similar PCEs implied that the obtained $CsPbBr_3$ layers with monolayer-vertical

structures have long carrier diffusion lengths. In our previous study, thick $CsPbBr_3$ films prepared by the mist deposition method demonstrated a high carrier mobility (13 $cm^2\ V^{-1}\ s^{-1}$) and a low trap density ($1.3 \times 10^{12}\ cm^{-3}$), which are comparable to those for single crystals.[32] For $CsPbBr_3$ single crystals, the diffusion lengths for electrons and holes have been reported to be 10.9 and 9.5 μm, respectively,[34] and therefore this speculation seems reasonable. It should be noted that there was no significant degradation of ITO performance including conductivity and transmittance because the annealing time was short in this study.

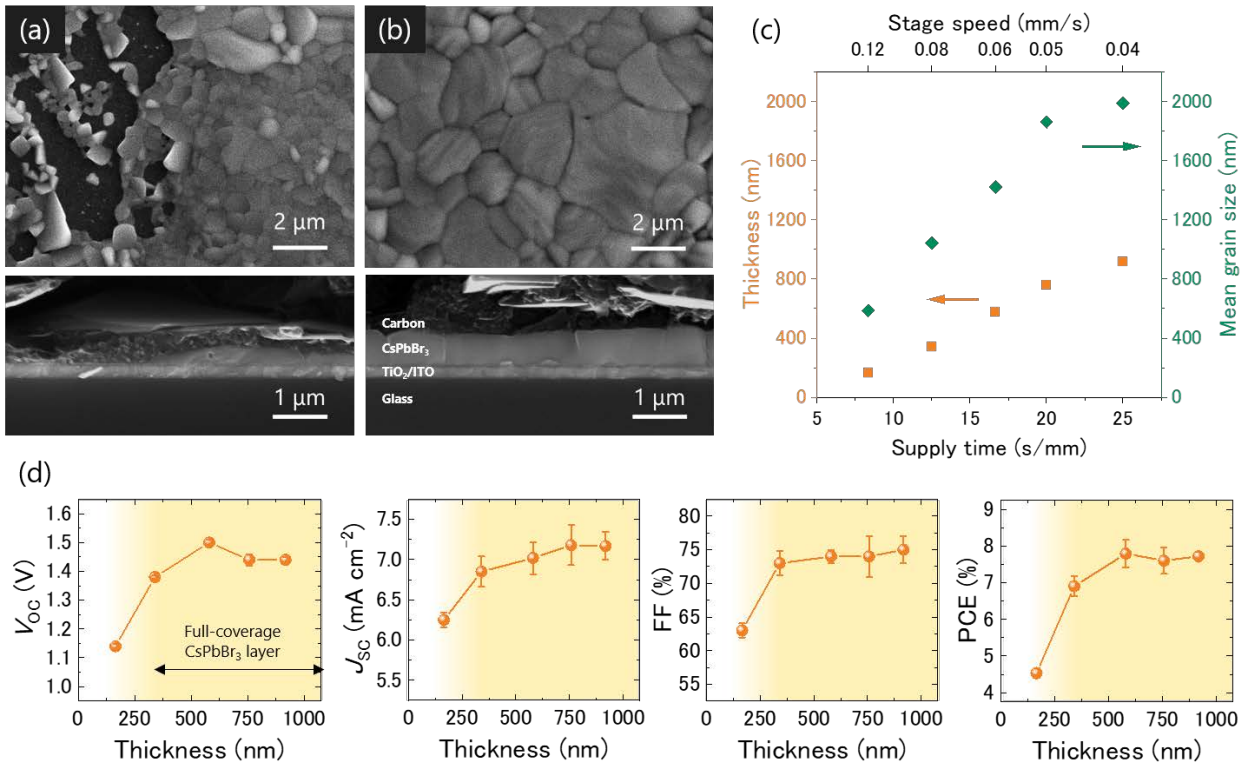


**Figure 3.** (a, b) Surface and cross-sectional SEM images of $CsPbBr_3$ PSCs with $CsPbBr_3$ layer deposited at stage speeds of (a) 0.12, and (b) 0.06 mm $s^{-1}$, respectively. (c) Correlation between supply time, film thickness, and mean grain size. (d) Photovoltaic performance, including $J_{SC}$, $V_{OC}$, FF, and PCE, of the $CsPbBr_3$ PSCs with $CsPbBr_3$ layers of various thicknesses.

Figure 4a shows the current density–voltage (*J*–*V*) curve of a typical 580 nm $CsPbBr_3$-based PSC, for which the corresponding photovoltaic parameters were a PCE of 8.3%, a $J_{SC}$ of 7.3 mA $cm^{-2}$, a $V_{OC}$ of 1.51 V, and a FF of 0.75. To evaluate the validity of the photovoltaic performance of our devices, the stabilized current density and PCE were measured at a bias voltage of 1.27 V. As shown in Figure 4b, the current density and PCE gradually increased and stabilized at 6.1 mA $cm^{-2}$ and 7.7%, respectively. The stabilized PCE of 7.7% is the highest reported value for carbon-based $CsPbBr_3$ PSCs prepared via a one-step solution process. The full surface coverage and large grain size of the $CsPbBr_3$ layer seem to contribute to this excellent performance. In comparison to state-of-the-art $CsPbBr_3$ PSCs prepared via two-step solution processes (Table S1), the stabilized PCE of 7.7% is still low but comparable to control devices without any interface engineering. Considering that our devices suffered from hysteresis (Figure S8), which is related to the defects and trap states at the perovskite/adjacent layer interface,[35] it is expected that interface engineering can eliminate hysteresis and further improve the PCE.[12–17] To evaluate the reproducibility of our mist deposition method for $CsPbBr_3$ PSCs, we fabricated 18 cells and measured their PCEs. As shown by the histogram in Figure 4c, the PCEs were distributed over a small range with an average value of 7.7% and a standard deviation of 0.6%, suggesting high reproducibility. The $CsPbBr_3$ PSC can maintain 84% of its initial PCE values under continuous light illumination over 10000 s (Figure 4d). Additionally, even after more than two months of storage in atmospheric conditions (0–25 °C, average RH 60%) without any encapsulation, there was no degradation of photovoltaic performance (Figure 4e).

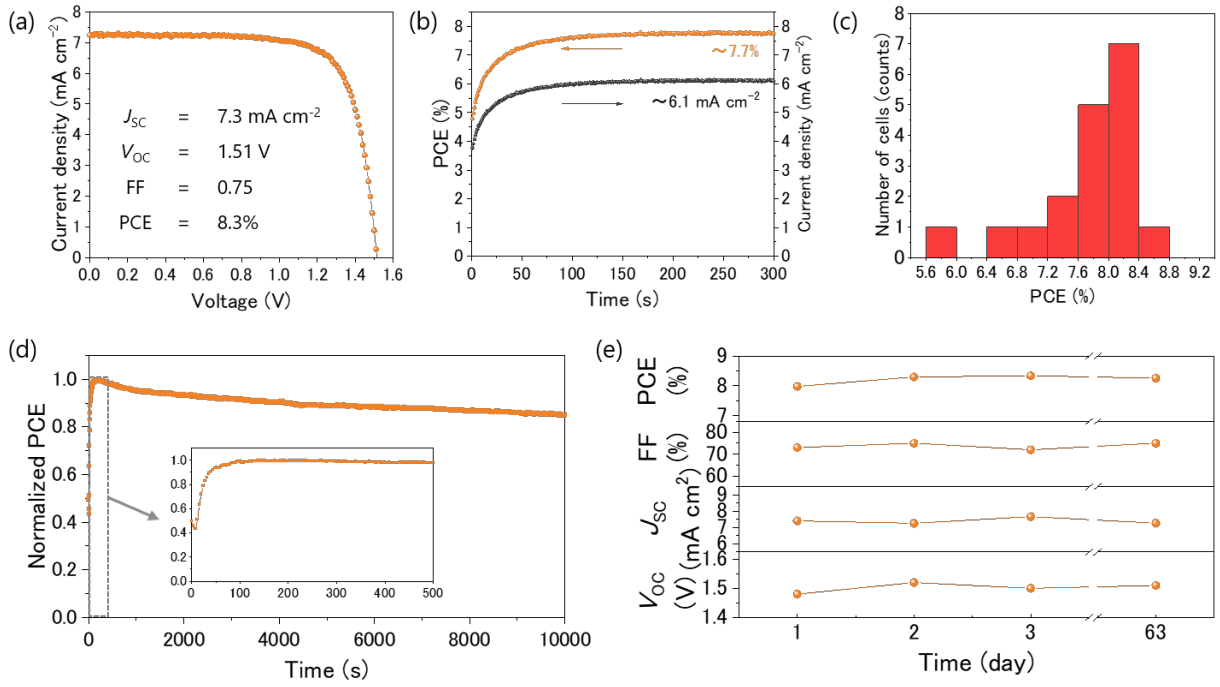


**Figure 4.** (a) *J–V* curve of a typical $CsPbBr_3$ PSC. (b) Stabilized PCE and current density at a bias voltage of 1.27 V. (c) Histogram of the PCEs of 18 $CsPbBr_3$ PSCs. (d) Photostability and (e) storage stability of $CsPbBr_3$ PSCs without any encapsulation.

In summary, we demonstrated the fabrication of a one-step solution-processed $CsPbBr_3$ PSCs using a mist deposition method. $CsPbBr_3$ films with full surface coverage and a large grain size were obtained at thicknesses of more than 340 nm, whereas thinner $CsPbBr_3$ films suffered from poor coverage. The 580 nm $CsPbBr_3$-based device achieved an excellent photovoltaic performance, including a PCE of 8.3%, a $J_{SC}$ of 7.3 mA cm$^{-2}$, a $V_{OC}$ of 1.51 V, and a FF of 0.75. Moreover, the stabilized PCE of 7.7% is the highest value for a $CsPbBr_3$-based PSC fabricated via a one-step solution process and is comparable to those for PSCs fabricated via two-step solution processes. Notably, the PCE of the $CsPbBr_3$ PSC decreased by only 0.1% on increasing the thickness of the $CsPbBr_3$ layer from 580 to 920 nm, suggesting that our $CsPbBr_3$ layers had a long carrier diffusion length. The full surface coverage and micrometer-order grain size of the $CsPbBr_3$ layer seem to

contribute to this excellent performance. Our future work will focus on using interface engineering to further improve the overall performance of carbon-based $CsPbBr_3$ PSCs. We expect that the findings of this study will accelerate the industrialization of $CsPbBr_3$ PSCs.

## ASSOCIATED CONTENT

Supporting Information Available: Experimental details, solvent viscosity and $CsPbBr_3$ solubility, optical characteristics and SEM images of $CsPbBr_3$ films, hysteresis of carbon-based $CsPbBr_3$ PSC, and photovoltaic performance of representative carbon-based $CsPbBr_3$ PSCs.

## AUTHOR INFORMATION

*E-mail: ikenoue.takumi.4m@kyoto-u.ac.jp

### Notes

The authors declare no competing financial interest.

## ACKNOWLEDGMENT

This work was supported by Hamamatsu Photonics K. K. and JSPS KAKENHI (Grant No. 18K18943).

## REFERENCES

(1) Kojima, A.; Teshima, K.; Shirai, Y.; Miyasaka, T. Organometal Halide Perovskites as Visible-Light Sensitizers for Photovoltaic Cells. *J. Am. Chem. Soc.* **2009**, *131* (17), 6050–6051.

(2) Eperon, G. E.; Stranks, S. D.; Menelaou, C.; Johnston, M. B.; Herz, L. M.; Snaith, H. J. Formamidinium Lead Trihalide: A Broadly Tunable Perovskite for Efficient Planar Heterojunction Solar Cells. *Energy Environ. Sci.* **2014**, *7* (3), 982.

(3) Dong, Q.; Fang, Y.; Shao, Y.; Mulligan, P.; Qiu, J.; Cao, L.; Huang, J. Electron-Hole Diffusion Lengths > 175 μm in Solution-Grown $CH_3NH_3PbI_3$ Single Crystals. *Science (80-. ).* **2015**, *347* (6225), 967–970.

(4) Jena, A. K.; Kulkarni, A.; Miyasaka, T. Halide Perovskite Photovoltaics: Background, Status, and Future Prospects. *Chem. Rev.* **2019**, *119* (5), 3036–3103.

(5) Fu, R.; Zhou, W.; Li, Q.; Zhao, Y.; Yu, D.; Zhao, Q. Stability Challenges for Perovskite Solar Cells. *ChemNanoMat* **2019**, *5* (3), 253–265.

(6) Kulbak, M.; Cahen, D.; Hodes, G. How Important Is the Organic Part of Lead Halide Perovskite Photovoltaic Cells? Efficient $CsPbBr_3$ Cells. *J. Phys. Chem. Lett.* **2015**, *6* (13), 2452–2456.

(7) Kulbak, M.; Gupta, S.; Kedem, N.; Levine, I.; Bendikov, T.; Hodes, G.; Cahen, D. Cesium Enhances Long-Term Stability of Lead Bromide Perovskite-Based Solar Cells. *J. Phys. Chem. Lett.* **2016**, *7* (1), 167–172.

(8) Ku, Z.; Rong, Y.; Xu, M.; Liu, T.; Han, H. Full Printable Processed Mesoscopic $CH_3NH_3PbI_3/TiO_2$ Heterojunction Solar Cells with Carbon Counter Electrode. *Sci. Rep.* **2013**, *3* (1), 3132.

(9) Mei, A.; Li, X.; Liu, L.; Ku, Z.; Liu, T.; Rong, Y.; Xu, M.; Hu, M.; Chen, J.; Yang, Y.; Grätzel, M.; Han, H. A Hole-Conductor-Free, Fully Printable Mesoscopic Perovskite Solar Cell with High Stability. *Science (80-. ).* **2014**, *345* (6194), 295–298.

(10) Hu, Y.; Si, S.; Mei, A.; Rong, Y.; Liu, H.; Li, X.; Han, H. Stable Large-Area (10 × 10 $cm^2$) Printable Mesoscopic Perovskite Module Exceeding 10% Efficiency. *Sol. RRL* **2017**, *1* (2), 2–7.

(11) Liang, J.; Wang, C.; Wang, Y.; Xu, Z.; Lu, Z.; Ma, Y.; Zhu, H.; Hu, Y.; Xiao, C.; Yi, X.; Zhu, G.; Lv, H.; Ma, L.; Chen, T.; Tie, Z.; Jin, Z.; Liu, J. All-Inorganic Perovskite Solar Cells. *J. Am. Chem. Soc.* **2016**, *138* (49), 15829–15832.

(12) Tang, Q.; Duan, J.; Zhao, Y.; He, B. High-Purity Inorganic Perovskite Films for 9.72%-Efficiency Solar Cells. *Angew. Chemie Int. Ed.* **2018**, *57*, 1–6.

(13) Liu, Z.; Sun, B.; Liu, X.; Han, J.; Ye, H.; Shi, T.; Tang, Z.; Liao, G. Efficient Carbon-Based $CsPbBr_3$ Inorganic Perovskite Solar Cells by Using Cu-Phthalocyanine as Hole Transport Material. *Nano-Micro Lett.* **2018**, *10* (2), 34.

(14) Ding, J.; Duan, J.; Guo, C.; Tang, Q. Toward Charge Extraction in All-Inorganic Perovskite Solar Cells by Interfacial Engineering. *J. Mater. Chem. A* **2018**, *6* (44), 21999–22004.

(15) Duan, J.; Zhao, Y.; Wang, Y.; Yang, X.; Tang, Q. Hole-Boosted $Cu(Cr,M)O_2$ Nanocrystals for All-Inorganic $CsPbBr_3$ Perovskite Solar Cells. *Angew. Chemie Int. Ed.* **2019**, *58* (45), 16147–16151.

(16) Duan, J.; Wang, Y.; Yang, X.; Tang, Q. Alkyl-Chain-Regulated Charge Transfer in Fluorescent Inorganic $CsPbBr_3$ Perovskite Solar Cells. *Angew. Chemie Int. Ed.* **2020**, *59* (11), 4391–4395.

(17) Tang, Q.; Zhou, Q.; Duan, J.; Yang, X.; Duan, Y. Interfacial Strain Release from $WS_2/CsPbBr_3$ van Der Waals Heterostructure for 1.7 V-Voltage All-Inorganic Perovskite Solar Cells. *Angew. Chemie* **2020**, 1–6.

(18) Li, Y.; Duan, J.; Yuan, H.; Zhao, Y.; He, B.; Tang, Q. Lattice Modulation of Alkali Metal Cations Doped $Cs_{1-x}R_xPbBr_3$ Halides for Inorganic Perovskite Solar Cells. *Sol. RRL* **2018**, *2* (10), 1800164.

(19) Yuan, H.; Zhao, Y.; Duan, J.; Wang, Y.; Yang, X.; Tang, Q. All-Inorganic $CsPbBr_3$ Perovskite Solar Cell with 10.26% Efficiency by Spectra Engineering. *J. Mater. Chem. A* **2018**, *6* (47), 24324–24329.

(20) Tang, M.; He, B.; Dou, D.; Liu, Y.; Duan, J.; Zhao, Y.; Chen, H.; Tang, Q. Toward Efficient and Air-Stable Carbon-Based All-Inorganic Perovskite Solar Cells through Substituting $CsPbBr_3$ Films with Transition Metal Ions. *Chem. Eng. J.* **2019**, *375* (June), 121930.

(21) Wang, Z.; Luo, Z.; Zhao, C.; Guo, Q.; Wang, Y.; Wang, F.; Bian, X.; Alsaedi, A.; Hayat, T.; Tan, Z. Efficient and Stable Pure Green All-Inorganic Perovskite $CsPbBr_3$ Light-Emitting Diodes with a Solution-Processed $NiO_x$ Interlayer. *J. Phys. Chem. C* **2017**, *121* (50), 28132–28138.

(22) Song, L.; Guo, X.; Hu, Y.; Lv, Y.; Lin, J.; Liu, Z.; Fan, Y.; Liu, X. Efficient Inorganic Perovskite Light-Emitting Diodes with Polyethylene Glycol Passivated Ultrathin $CsPbBr_3$ Films. *J. Phys. Chem. Lett.* **2017**, *8* (17), 4148–4154.

(23) Ren, Y.; Hao, Y.; Zhang, N.; Arain, Z.; Mateen, M.; Sun, Y.; Shi, P.; Cai, M.; Dai, S. Exploration of Polymer-Assisted Crystallization Kinetics in $CsPbBr_3$ All-Inorganic Solar Cell. *Chem. Eng. J.* **2019**, 123805.

(24) Dirin, D. N.; Cherniukh, I.; Yakunin, S.; Shynkarenko, Y.; Kovalenko, M. V. Solution-Grown $CsPbBr_3$ Perovskite Single Crystals for Photon Detection. *Chem. Mater.* **2016**, *28* (23), 8470–8474.

(25) Park, M.; Cho, W.; Lee, G.; Hong, S. C.; Kim, M.; Yoon, J.; Ahn, N.; Choi, M. Highly Reproducible Large-Area Perovskite Solar Cell Fabrication via Continuous Megasonic Spray Coating of $CH_3NH_3PbI_3$. *Small* **2019**, *15* (1), 1804005.

(26) Chen, H.; Ding, X.; Pan, X.; Hayat, T.; Alsaedi, A.; Ding, Y.; Dai, S. Comprehensive Studies of Air-Brush Spray Deposition Used in Fabricating High-Efficiency $CH_3NH_3PbI_3$ Perovskite Solar Cells: Combining Theories with Practices. *J. Power Sources* **2018**, *402*, 82–90.

(27) Heo, J. H.; Lee, M. H.; Jang, M. H.; Im, S. H. Highly Efficient $CH_3NH_3PbI_{3-x}Cl_x$ Mixed Halide Perovskite Solar Cells Prepared by Re-Dissolution and Crystal Grain Growth via Spray Coating. *J. Mater. Chem. A* **2016**, *4* (45), 17636–17642.

(28) Bhachu, D. S.; Scanlon, D. O.; Saban, E. J.; Bronstein, H.; Parkin, I. P.; Carmalt, C. J.; Palgrave, R. G. Scalable Route to $CH_3NH_3PbI_3$ Perovskite Thin Films by Aerosol Assisted Chemical Vapour Deposition. *J. Mater. Chem. A* **2015**, *3* (17), 9071–9073.

(29) Ikenoue, T.; Sakamoto, S.; Inui, Y. Fabrication and Characterization of $Cu_2O$, ZnO and ITO Thin Films toward Oxide Thin Film Solar Cell by Mist Chemical Vapor Deposition Method. *Phys. status solidi* **2014**, *11* (7–8), 1237–1239.

(30) Kawaharamura, T.; Nishinaka, H.; Kamaka, Y.; Masuda, Y.; Lu, J.-G.; Fujita, S. Mist CVD Growth of ZnO-Based Thin Films and Nanostructures. *J. Korean Phys. Soc.* **2008**, *53* (9(5)), 2976–2980.

(31) Stoumpos, C. C.; Malliakas, C. D.; Peters, J. A.; Liu, Z.; Sebastian, M.; Im, J.; Chasapis, T. C.; Wibowo, A. C.; Chung, D. Y.; Freeman, A. J.; Wessels, B. W.; Kanatzidis, M. G. Crystal Growth of the Perovskite Semiconductor $CsPbBr_3$ : A New Material for High-Energy Radiation Detection. *Cryst. Growth Des.* **2013**, *13* (7), 2722–2727.

(32) Haruta, Y.; Ikenoue, T.; Miyake, M.; Hirato, T. Fabrication of (101)-Oriented $CsPbBr_3$ Thick Films with High Carrier Mobility Using a Mist Deposition Method. *Appl. Phys. Express* **2019**, *12* (8), 085505.

(33) Fu, K.; Nelson, C. T.; Scott, M. C.; Minor, A.; Mathews, N.; Wong, L. H. Influence of Void-Free Perovskite Capping Layer on the Charge Recombination Process in High Performance $CH_3NH_3PbI_3$ Perovskite Solar Cells. *Nanoscale* **2016**, *8* (7), 4181–4193.

(34) Song, J.; Cui, Q.; Li, J.; Xu, J.; Wang, Y.; Xu, L.; Xue, J.; Dong, Y.; Tian, T.; Sun, H.; Zeng, H. Ultralarge All-Inorganic Perovskite Bulk Single Crystal for High-Performance Visible-Infrared Dual-Modal Photodetectors. *Adv. Opt. Mater.* **2017**, *5* (12), 1700157.

(35) Chen, B.; Yang, M.; Priya, S.; Zhu, K. Origin of J – V Hysteresis in Perovskite Solar Cells. *J. Phys. Chem. Lett.* **2016**, *7* (5), 905–917.